Northumbria Research Link

**ADVANCED
SCIENCE NEWS**

www.advancedsciencenews.com

**ADVANCED
OPTICAL
MATERIALS**

www.advopticalmat.de

COMMUNICATION

Toward Direct Laser Writing of Actively Tuneable 3D Photonic Crystals

Yaoyang Hu, Benjamin T. Miles, Ying-Lung D. Ho, Mike P. C. Taverne, Lifeng Chen, Henkjan Gersen, John G. Rarity, and Charl F. J. Faul*

Actively tuneable optical systems are evolving as an important research field,[1] enabling the formation of adaptable structures for application as displays[2] and sensing devices.[3,4] An ideal actively tuneable optical system would be characterized by a high response rate, could be reversibly tuned, and be miniaturized for integration into existing photonic devices.[5] Owing to the simplicity of their structure and fabrication, and the predictability of their optical properties, the most common tuneable optical systems are 1D photonic crystals.[6,7] Self-assembly approaches to 3D periodic structures (using colloidal spheres immersed in liquids or embedded in polymers[8,9]) have shown significant promise for tuneable color and strain sensing. However, direct write fabrication brings the flexibility to engineer arbitrary structures such as tuneable lenses,[10,11] and produce a series of 2D and 3D tuneable optical systems that are optically active over a wide wavelength range.[12–15]

Currently, many routes to tuneable optical systems exploit mechanisms such as swelling of the optical material,[3,10] thermally controlled dimensional changes,[5] or interaction between solvents and optical structures.[7,10] The focus of this study is on using materials that undergo refractive index changes (and tuning), induced by a chemical reaction that transfers the materials from a dielectric to a conducting state. Under this approach the material does not undergo any changes in geometry or dimensions. This allows the optical system to maintain its structure which will, in principle, lead to many reversible tuning cycles.

An attractive class of addressable material for this purpose is organic semiconductors: versatile materials that offer tuneable functionality, including charge transport and switchable

Y. Hu, Prof. C. F. J. Faul
School of Chemistry
University of Bristol
Cantock's Close, Bristol BS8 1TS, UK
E-mail: charl.faul@bristol.ac.uk
Dr. B. T. Miles, Dr. H. Gersen
H. H. Wills Physics Laboratory
University of Bristol
Tyndall Avenue, Bristol BS8 1TL, UK
Dr. Y.-L. D. Ho, M. P. C. Taverne, Dr. L. Chen, Prof. J. G. Rarity
Department of Electrical and Electronic Engineering
University of Bristol
Bristol BS8 1TR, UK

optoelectronic properties.[16] These features have already been used in a wide range of (well-known) applications, including photovoltaics,[17] printable flexible organic electronics,[18] supercapacitors, and rechargeable batteries.[19] However, their conjugated architectures can lead to poor solubility and processability. The oligomer approach[20] has provided a promising route to improve processability and provides well-defined and tuneable molecular architectures whilst maintaining the properties of the parent polymer. This approach has been exploited for a number of well-known electroactive polymers, including poly(thiophene)s, poly(phenylenevinylene), and more recently, also for poly(aniline). Our efforts have been focused on the design and syntheses of well-defined oligo(aniline)-based materials.[16] The self-assembly and tuneable optoelectronic properties of these attractive materials have been exploited[21] using their well-known switchable oxidation states: the fully reduced gray leucoemeraldine base (LEB) state, the half-oxidized blue-purple emeraldine base (EB) state, and the doped and conducting green emeraldine salt (ES) state.[22] The ability to easily access the conducting ES state through acid–base doping provides the possibility to fabricate functional supramolecular assemblies,[23,24] especially when using different acid dopants.[25] It has also been shown that additional modification of the molecular architectures is possible through variation of the terminal amine groups.[26]

Here the first steps toward tuneable optical elements achieved through direct laser writing (DLW) of addressable oligo(aniline)-based material on the appropriate length scales, with the required 2D and 3D geometries for use in optical chip technologies, are shown. In the DLW approach a 2-photon polymerization (2PP) process is initiated by focusing a laser, here a pulsed erbium-doped femtosecond fiber laser source ($\lambda \approx 780$ nm), into a thin film of a photoresist. A 3D structure is written within the pathway of laser focus (i.e., negative tone photoresist) as it is scanned through the material. Structures can be prepared with a resolution of less than 100 nm.[27] This technique can be easily integrated with existing optical devices, such as lab-on-a-chip systems and functional biomedical devices to achieve miniaturized optical chip platforms.[3] DLW furthermore enables testing of custom designs,[28] as it does not require exposure to high temperature or highly acidic environments, which are commonly found in other fabrication approaches.[29]

As discussed previously, a material with a switchable refractive index without geometric modification is desired. Here, for the first time, the synthesis of a novel material (Boc-**TANIDA**) that can be used to fabricate nanoscale 2D/3D structures with a switchable refractive index and a negligible corresponding dimensional change using DLW is shown. Boc-**TANIDA** was synthesized by

ADVANCED
OPTICAL
MATERIALS
www.advopticalmat.de

ADVANCED
SCIENCE NEWS
www.advancedsciencenews.com

COMMUNICATION

Scheme 1. Procedure for the synthesis of Boc-**TANIDA**. a) *p*-Nitrofluorobenzene, Et$_3$N, DMSO, under N$_2$, 90 °C, 24 h, yield 69%, b) Di-*t*-butyl dicarbonate (Boc), 4-(dimethylamino)pyridine, dry THF, under N$_2$, 65 °C, reflux, 24 h, yield 83%, c) Pd/C, ammonium formate, dry methanol, dry THF, under N$_2$, 65 °C, reflux, 5 h, yield 78%, d) acryloyl chloride, Et$_3$N, dry THF, under N$_2$, rt, 2 h, yield 86%. See Supporting Information for all experimental and analytical details.

functionalizing NH$_2$/NH$_2$-capped tetra(aniline) (TANI) with photopolymerizable acrylate moieties (**Scheme 1**, with additional details in Supporting Information, Sections S1 and S2).

In brief, NH$_2$/NH$_2$ TANI was synthesized by a S$_N$Ar coupling of fluoro-*p*-nitrobenzene with diaminodiphenylamine to yield intermediate **2**.[30,31] After Boc-protection of the secondary amines (**3**), reduction of the NO$_2$ groups yielded the desired product **4**.[32] The photopolymerizable acrylate group was attached to **TANI** using a standard acylation reaction (details in Supporting Information, Sections S1 and S2), to yield *tert*-butyl (4-acrylamidophenyl)(4-((4-((4-acrylamidophenyl)(tert-butoxycarbonyl)amino)phenyl)(tert-butoxycarbonyl)amino) phenyl)-carbamate, Boc-**TANIDA**, in a modest overall yield. Our Boc-protection strategy is important for two reasons: (1) to ensure that a transparent film of good quality is obtained for 2PP, and (2) Boc-protection furthermore fixes the aniline N atoms in the LEB state, thus preventing them from

taking part in the well-known redox-activity of the parent TANI, which would otherwise inhibit radical polymerization.[33]

Building on the successful precursor synthesis, initial investigations focused on the preparation of simple **TANIDA**-based structures to achieve a number of key objectives: (1) to optimize DLW operating parameters, determine voxel size, and thus ensure the production/writing of mechanically stable nanostructured architectures; (2) to explore deprotection strategies of the written structures, allowing access to the attractive switchable features of our aniline-based materials; and (3) to determine the effect of oxidation state and doping on the refractive index of the photopolymerized material.

In order to ensure that the 2PP process would proceed with high efficiency, the optical absorption of the materials was measured to confirm their compatibility with the process. **Figure 1**a shows the UV–vis spectra of Boc-**TANIDA**, trimethylolpropane triacrylate (TMPTA) cross-linker, and
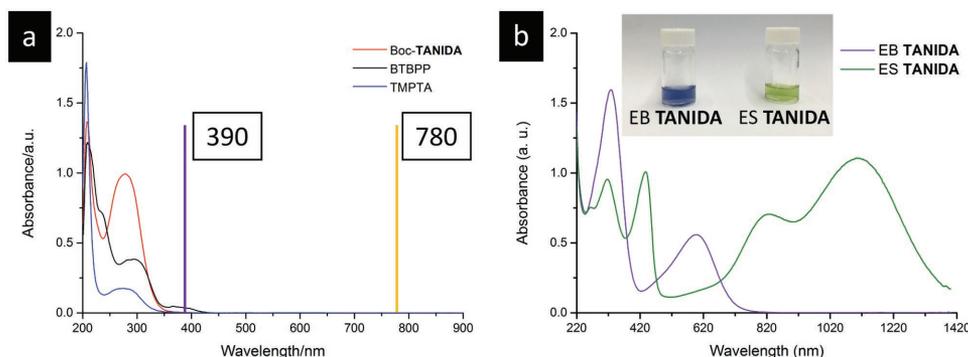
Figure 1. a) UV–vis spectra of Boc-**TANIDA**, BTBPP, and TMPTA compared with the laser beam wavelength at 780 nm and 2-photon absorption at 390 nm, thus showing compatibility of the material used with 2PP. If deprotected, oligo(aniline)s exhibit the same distinct three redox states found for the parent polymer poly(aniline) (gray fully reduced LEB state, blue half-oxidized EB state, and the green doped conducting ES state). b) The typical UV–vis spectra of EB **TANIDA** and ES **TANIDA** in ethanol solution (2 × 10^{-5} M), with the distinctive long-wavelength absorption features found for the doped ES state.

bis(2,4,6-trimethylbenzoyl)-phenyl phosphineoxide (BTBPP) photoinitiator, respectively. The materials show no absorption above 450 nm, which provides a wide transparency window for the incident laser beam at 780 nm (Figure 1b). Furthermore, only BTBPP absorbs at 390 nm, thus ensuring efficient initiation of the 2PP process at this wavelength.

A photoactive functional formulation was optimized (56 wt% Boc-**TANIDA**, 40 wt% TMPTA cross-linker, and 4 wt% BTBPP photoinitiator in dichloromethane) to prepare high quality transparent thin films for DLW (see Supporting Information, Section S3, for full details of the optimization process and scanning electron microscopy (SEM) images of structures printed from the various formulations). The optimized formulation was drop cast on a glass substrate (22 mm × 22 mm), attached to a sample holder and 20 µm × 20 µm block structures were written (Nanoscribe, 6 mW laser power and 100 µm s^{-1} scan speed, detail in Supporting Information, Section S3). After polymerization, the surface-anchored 2D structures were developed in isopropanol, and all unpolymerized Boc-**TANIDA** monomers removed.

With the monomer formulation and polymerization procedures optimized, a range of simple 2D and increasing complex and intricate 3D structures, such as the face-centered cubic (FCC) woodpile structure shown in **Figure 2**a (see Figure S7 of the Supporting Information for further examples) were printed. The dimensions of the woodpile structure are 50 µm × 50 µm × 10 µm, with voxel size determined to be ≈260 nm × 260 nm × 960 nm (see Supporting Information, Sections S4 and S5, and accompanying figures, for details of the design and voxel size determination).

Directly after DLW of structures, the **TANIDA** backbones were still Boc-protected, thus hindering any attempts at switching oxidation or conductive state. The first step, once 3D printed structures were demonstrated, was to ensure deprotection and

efficient removal of these groups. Woodpile structures were heated to 140 °C for 18 h in a nitrogen atmosphere, thus fully ensuring thermolysis and removal of all Boc groups. This procedure left the **TANIDA**-based photopolymerized structures in the fully reduced LEB state. The structures were subsequently oxidized to the EB state by submerging them in a 5% H_2O_2 aqueous solution, and the ES state obtained by exposing the EB-state structure to HCl vapor (Figure 2c). Exposing this 2PP-written 3D woodpile structure to doping (HCl) and dedoping (NH₃) cycles confirmed a homogenous and reversible color change. Reflectance spectra show a change in the reflected intensity as well as a change in the number of interference fringes between the EB and ES state of the woodpile structure (Figure 2b), which both indicate a change in the refractive index. This well-known acid-base doping/dedoping cycle could easily be repeated (up to five times, before formation of NH₄Cl on the printed structure was observed; see Figure S10 of the Supporting Information for details) without degradation of the DLW structures. The 3D structure as a whole undergoes the expected changes without any noticeable distortion; the switchable behavior was therefore explored for photonic applications.

To use our new material in photonic applications it is crucial to not only show (macroscopically) reversible behavior, but, more importantly, to determine the refractive index for both the doped and de-doped state. In general, the optical delay experienced upon propagation through a material is a function of both the refractive index and the thickness of a material, hence both these parameters have to be determined. Measuring the refractive index by standard ellipsometry proved infeasible in our case, as depositing thin films with a homogeneous thickness for these materials on the required length-scales to perform this technique proved experimentally challenging.

To circumvent these experimental difficulties and measure the refractive indices in situ, a microscale wedge-shaped
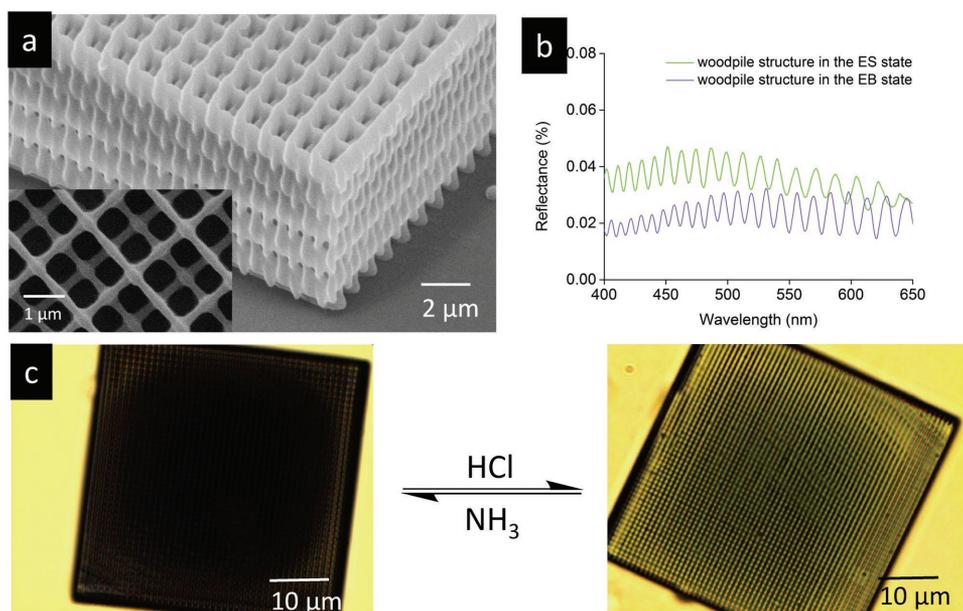

Figure 2. a) 2PP-printed FCC woodpile structures. b) Reflectance spectra of a woodpile structure in the EB and ES state. c) Optical images showing the induced color changes during the doping/dedoping process. See Figure S7 of the Supporting Information for additional printed structures.

**ADVANCED
OPTICAL
MATERIALS**
www.advopticalmat.de

**ADVANCED
SCIENCE NEWS**
www.advancedsciencenews.com

COMMUNICATION
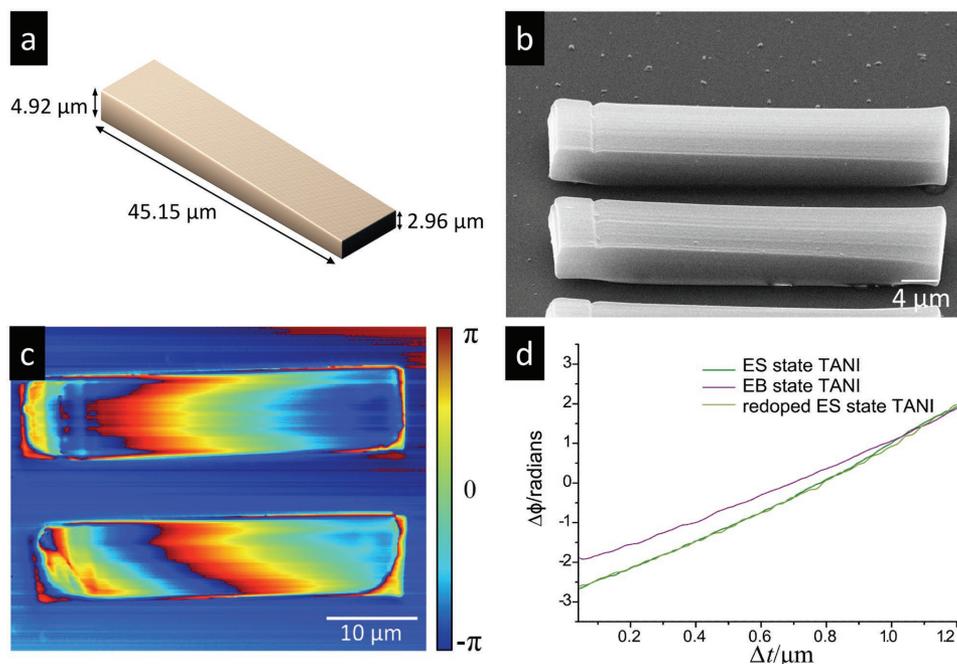
Figure 3. a) Structural design and dimensions of the wedge shapes. b) SEM image of wedge structures written by 2PP. c) The change in optical phase showing the written optical wedges, combined with the measured height of the structure, which provides a direct measurement of the refractive index for both of the doped and dedoped state. d) Phase profile as a function of thickness for doped, dedoped, and redoped wedge structures (i.e., one full cycle), normalized to a common maximum phase value for readability. This shows that the refractive index change is fully reversible. See detailed discussion in the text and the Supporting Information.

structure was designed that increased in thickness from 2.96 to 4.92 µm over a total length of 45 µm (see **Figure 3**a). After fabrication, the wedge structures showed heights from 3.39 to 5.65 µm over a total length of 42.43 µm. The smaller lateral size can be explained by shrinkage during the developing process. The different vertical size between the design and fabricated wedge structure is due to a combination of the following factors: (a) the accuracy of finding the glass/photoresist interface; (b) the vertical stage positioning precision; (c) the shrinkage during developing and (d) the voxel size and actual Z position changing with the designed Z position (caused by the refractive index mismatch between the photoresist and the glass substrate). The effects of (c) and (d) could be reduced by further calibrating the input file used in the 2PP process. This approach (i.e., the in situ measurement of a custom-designed wedge shape) enabled us to measure the optical delay in an imaging-type Mach–Zehnder interferometer[34,35] for a structure where the amount of additional material as a function of position is known.

By writing a wedge structure with a smooth thickness gradient, rather than a sample with discrete height jumps, continuous phase delay information from the structure could be extracted without risking the phase degenerately wrapping over 2π. This sample was placed in one branch of an imaging-type Mach–Zehnder interferometer, capable of detecting both amplitude and phase and illuminated using a 532 nm laser. Imaging the wedge-shaped samples reports on both the optical absorption and phase delay as a function of position, which directly correlates with sample thickness. Using the known thickness as determined by SEM and the known optical wavelength (from

the laser), allowed us to determine the optical delay experienced with respect to propagation through free space. This approach provides a direct measurement of the refractive indices (Equation (1)), where n is refractive index, $\Delta\psi$ is phase delay as the function of position, λ is the laser wavelength, and Δt is the thickness difference

$$n = \frac{\Delta\psi \times \lambda}{\Delta t \times 2\pi} + 1 \tag{1}$$

From the thickness, optical wavelength, and phase delay, a refractive index of $n = 1.332 \pm 0.001$ was determined for the doped structures. After exposing the structures to ammonia gas for 5 min and reimaging, a change in the refractive index of 0.047 to $n = 1.285 \pm 0.007$ was measured for the dedoped structures.

To prove that the materials are addressable and that the change in refractive index is fully reversible, the structure were exposed to HCl gas for 5 min, reimaged, and showed switching of the refractive index back to $n = 1.332$. Figure 3d shows the line trace of measured phase delay as a function of sample thickness over the first wedge structure for a single cycle. These traces have been normalized to coincide at a common maxima for readability and display excellent agreement between the doped and redoped states, with a lower gradient for the dedoped state corresponding to a lower refractive index. Minor variations in linearity of the slopes can be attributed to a slight inhomogeneity of the surface of the wedge as seen in Figure 3b (corresponding to height variations of <100 nm). Imaging of both doped and dedoped structures by SEM showed

no detectable changes in the physical dimensions of the ramps, confirming that the observed refractive index changes do not result from a change in physical dimensions of the written structure. In addition, modeling shows that the structures as written would induce a shift in the first order bandgap position from 2.03 to 1.99 μm (in air) for doped and dedoped structures, respectively, which was outside the detectable wavelength range here (see Supporting Information, Section S8 for details).

In conclusion, a simple approach toward the design and direct writing of stable 3D photonic structures with reversibly addressable refractive indices using polymerizable redox-active materials has been shown. The switchability, high surface-to-volume ratio, and opportunities for further chemical functionalization of the intricate 3D surfaces, through simple dopant variations or surface chemical treatment, present a range of opportunities in sensing. However, other switching mechanisms would need to be explored, as the utilized chemical doping–dedoping cycles are limited to 5 due to the formation of ammonium chloride on the printed structures. Changing the doping/dedoping approach would also allow performing in situ doping–dedoping experiments, thus enabling further detailed time-dependent studies of this promising switching approach. Further optimization of the formulation and writing process to create bandgaps in the more technologically relevant telecommunications[36] window and at even shorter wavelengths are topics for future investigations currently being explored in our laboratories.

Supporting Information

Supporting Information is available from the Wiley Online Library or from the author.

Acknowledgements

[1] J. Ge, Y. Yin, *Angew. Chem. Int. Ed.* **2011**, *50*, 1492.

[2] J. J. Walish, Y. Kang, R. a. Mickiewicz, E. L. Thomas, *Adv. Mater.* **2009**, *21*, 3078.

[3] C. Fenzl, T. Hirsch, O. S. Wolfbeis, *Angew. Chem. Int. Ed.* **2014**, *53*, 3318.

[4] A. K. Yetisen, H. Butt, F. da Cruz Vasconcellos, Y. Montelongo, C. a. B. Davidson, J. Blyth, L. Chan, J. B. Carmody, S. Vignolini, U. Steiner, J. J. Baumberg, T. D. Wilkinson, C. R. Lowe, *Adv. Opt. Mater.* **2014**, *2*, 250.

[5] W. Zhang, K. Aljasem, H. Zappe, A. Seifert, *Opt. Express* **2011**, *19*, 9945.

[6] Y. Yue, J. P. Gong, *J. Photochem. Photobiol., C* **2015**, *23*, 45.

[7] Y. Kang, J. J. Walish, T. Gorishnyy, E. L. Thomas, *Nat. Mater.* **2007**, *6*, 957.

[8] M. G. Han, C. G. Shin, S.-J. Jeon, H.-S. Shim, C.-J. Heo, H. Jin, J. W. Kim, S.-Y. Lee, *Adv. Mater.* **2012**, *24*, 6438.

[9] C. I. Aguirre, E. Reguera, A. Stein, *Adv. Funct. Mater.* **2010**, *20*, 2565.

[10] D. Lu, Y. Zhang, D. Han, H. Wang, H. Xia, Q. Chen, H. Ding, H. Sun, *J. Mater. Chem. C* **2015**, *3*, 1751.

[11] L. Maigyte, V. Purlys, J. Trull, M. Peckus, C. Cojocaru, D. Gailevičius, M. Malinauskas, K. Staliunas, *Opt. Lett.* **2013**, *38*, 2376.

[12] D. McPhail, M. Straub, M. Gu, *Appl. Phys. Lett.* **2005**, *87*, 091117.

[13] A. M. Flatae, M. Burresi, H. Zeng, S. Nocentini, S. Wiegele, C. Parmeggiani, H. Kalt, D. Wiersma, *Light Sci. Appl.* **2015**, *4*, e282.

[14] Y. Montelongo, A. K. Yetisen, H. Butt, S.-H. Yun, *Nat. Commun.* **2016**, *7*, 12002.

[15] Y. Fang, Y. Ni, S.-Y. Leo, B. Wang, V. Basile, C. Taylor, P. Jiang, *Appl. Mater. Interfaces* **2015**, *7*, 23650.

[16] Z. Shao, P. Rannou, S. Sadki, N. Fey, D. M. Lindsay, C. F. J. Faul, *Chem. Eur. J.* **2011**, *17*, 12512.

[17] A. Teichler, J. Perelaer, U. S. Schubert, *J. Mater. Chem. C* **2013**, *1*, 1910.

[18] J. T. Muth, D. M. Vogt, R. L. Truby, Y. Mengüç, D. B. Kolesky, R. J. Wood, J. A. Lewis, *Adv. Mater.* **2014**, *26*, 6307.

[19] A. MacDiarmid, L. Yang, W. Huang, B. Humphrey, *Synth. Met.* **1987**, *18*, 393.

[20] K. Mullen, G. Wegner, *Electronic Materials: The Oligomer Approach*, Wiley-VCH, Weinheim, Germany **1998**.

[21] C. F. J. Faul, *Acc. Chem. Res.* **2014**, *47*, 3428.

[22] T. G. Dane, P. T. Cresswell, G. A. Pilkington, S. Lilliu, J. E. Macdonald, S. W. Prescott, O. Bikondoa, C. F. J. Faul, W. H. Briscoe, *Soft Matter* **2013**, *9*, 10501.

[23] O. A. Bell, G. Wu, J. S. Haataja, F. Brömmel, N. Fey, A. M. Seddon, R. L. Harniman, R. M. Richardson, O. Ikkala, X. Zhang, C. F. J. Faul, *J. Am. Chem. Soc.* **2015**, *137*, 14288.

[24] W. Lyu, J. Feng, W. Yan, C. F. J. Faul, *J. Mater. Chem. C* **2015**, *3*, 11945.

[25] T. G. Dane, P. T. Cresswell, O. Bikondoa, G. E. Newby, T. Arnold, C. F. J. Faul, W. H. Briscoe, *Soft Matter* **2012**, *8*, 2824.

[26] Z. Shao, Z. Yu, J. Hu, S. Chandrasekaran, D. M. Lindsay, Z. Wei, C. F. J. Faul, *J. Mater. Chem.* **2012**, *22*, 16230.

[27] G. Von Freymann, A. Ledermann, M. Thiel, I. Staude, S. Essig, K. Busch, M. Wegener, *Adv. Funct. Mater.* **2010**, *20*, 1038.

[28] H. Zeng, D. Martella, P. Wasylczyk, G. Cerretti, J.-C. G. Lavocat, C.-H. Ho, C. Parmeggiani, D. S. Wiersma, *Adv. Mater.* **2014**, *26*, 2319.

[29] M. A. Stanislav, P. E. Russell, *Nanofabrication Using Focused Ion and Electron Beams: Principles and Applications*, Oxford University Press, NY, USA **2012**.

[30] Z. Wei, C. F. J. Faul, *Macromol. Rapid Commun.* **2008**, *29*, 280.

[31] I. Kulszewicz-Bajer, I. Różalska, M. Kurłek, *New J. Chem.* **2004**, *28*, 669.

[32] R. Eelkema, H. L. Anderson, *Macromolecules* **2008**, *41*, 9930.

[33] R. Chen, B. Benicewicz, *Macromolecules* **2003**, *36*, 6333.

[34] X. Hong, E. M. P. H. van Dijk, S. R. Hall, J. B. Götte, N. F. van Hulst, H. Gersen, *Nano Lett.* **2011**, *11*, 541.

[35] B. T. Miles, X. Hong, H. Gersen, *Opt. Express* **2015**, *23*, 1232.

[36] L. Chen, M. P. C. Taverne, X. Zheng, J.-D. Lin, R. Oulton, M. Lopez-Garcia, Y.-L. D. Ho, J. G. Rarity, *Opt. Express* **2015**, *23*, 26565.